Partial power DC-DC converter to integrate PVs in DC grids

João Campos, MSc Student, IST; Sónia F. Pinto, Senior Member, IEEE and Guilherme M. Paraíso

***Abstract*—Partial power processing is a concept applied to power converters in order to reduce its losses, size and cost. This technique consists of designing a converter that only processes a fraction of the input power.**

This dissertation's objective is to analyze the performance of a partial power converter when operating in a DC microgrid. For that purpose, the partial power converter will be designed and sized to operate as both a step-up converter and a step-down converter to connect a PV system and a constant power load, respectively, to the DC microgrid.

A Maximum Power Point Tracker (MPPT) algorithm is used to guarantee maximum power generation of the PV system. For the converters, non-linear controllers were designed based on Lyapunov Stability Theory and used the Backstepping technique and Sliding Mode Control methods.

A DC microgrid was modelled and simulated and the results are analyzed to evaluate the performance of the DC microgrid components for different operation scenarios.

***Index Terms*— DC Microgrid, MPPT, Non-linear controllers, Partial Power Converter, PV system.**

I. Introduction

The technique of partial power processing consists of designing and sizing a converter to only process a fraction of the total power. This way the converter's losses, size and cost can be reduced. This technique is achieved by "splitting" the power flow into two paths: one being a series path between input and output and the other being the conversion stage. This way the conversion stage can be sized for a smaller power which means that in comparison to a full power converter its semiconductors ratings can be reduced. If it is the case that a transformer is used in the conversion stage, its rating and size can also be reduced. These improvements potentially lead to an increase in the converter's efficiency and a reduction of its size and cost.

The concept of Partial Power Converters (PPC) has been around for some time: in [1] a converter referred as Series Connect Boost Unit (SCBU) was presented for spacecraft applications. This converter achieved a high efficiency by using an isolated buck converter in series with the input voltage source which only processed a fraction of the total power. It must be noted that as more partial power processing architectures were presented along the years, the name SCBU became obsolete and many names have been used to refer to these types of converters, such as Partial Capacity Converter, Partial Power Processing Converters and Series Voltage Compensation [2]. This lack of agreement has been recognized in [3] and a unifying criteria for nomenclature has been proposed, however since it is out of the scope of this thesis to classify and analyze different PPC architectures the names of step-up and step-down PPC are chosen for simplicity.

More recently and focused in the problem of voltage mismatch between PV panels in a string (e.g. due to shading), presented in [4] is a study of various PV panel integrated DC-DC converters where the technique of PPC is analyzed as one of the solutions. Several applications have been proposed that follow this concept, such as: the well-known doubly fed induction generator [5] for wind turbines, a DC bus regulator [6] for spacecraft applications or a DC-DC converter [7] for distributed PV architectures. The topology that this thesis focuses on is the one in [2] and [8] in which a PPC based on a Flyback converter is presented to integrate two-stage configurations (a first DC-DC stage to boost the voltage and a second DC-AC stage to connect to the grid). For the purpose of this thesis only the DC-DC stage is interesting since the PV system is being connected to a DC grid instead of an AC grid.

II. DC Grid converters

The DC microgrid is composed of several converters, each with a different purpose. The focus of this thesis is the PPC topology that will be used to design two converters, a step-up converter and step-down converter. The step-up converter will be used to connect a single panel PV system to the DC microgrid whereas the step-down converter is used to connect Constant Power Loads (CPL) to the grid. The step-down converter is used to connect Constant Power Loads (CPL) to the grid. Lastly, a bidirectional Dual Active Bridge (DAB) converter is also used to set and maintain the DC microgrid voltage and to balance the power flow in the grid. These converters and the overall DC microgrid configuration can be seen in Fig. 1

1) Step-up Partial Power Converter

In order to connect the PV panel to the DC grid a step-up converter is needed to boost the voltage at the output of the panel. The DC grid operates at 380V while a 60 cell PV panel

voltage ranges around 30V, so a high voltage gain is required. A popular choice for this scenario is the flyback converter since it presents high voltage gain, galvanic isolation and it is used for low power (200-300W). The used PPC topology is based on the flyback converter and inherits most of its characteristics except galvanic isolation. A MOSFET semiconductor was chosen as the converter will operate at frequencies of 50 kHz and above. In Fig. 2 the PPC based on a flyback topology can be seen.

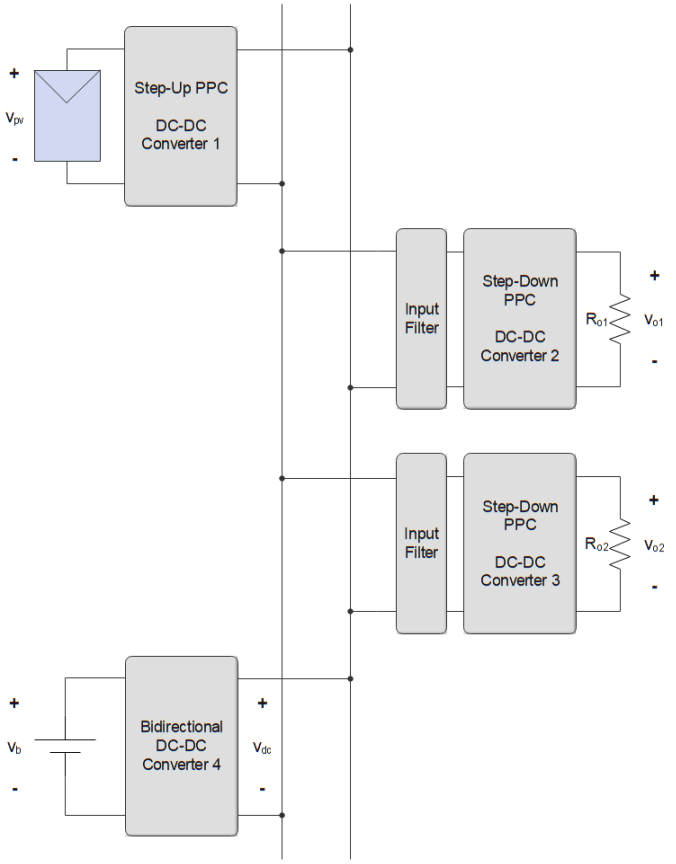

Fig. 1 - DC microgrid configuration

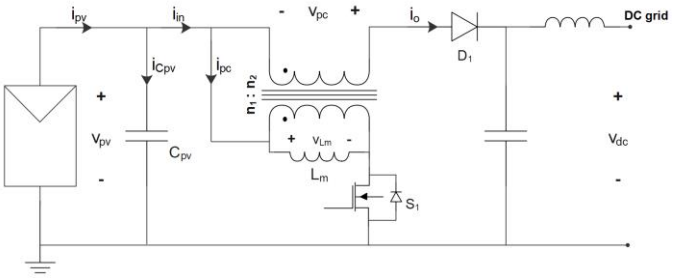

Fig. 2 - PV system connection to a DC grid using a flyback based partial power converter configuration

Applying Kirchhoff's laws we get (1) and (2):

$$V_{pv} + v_{pc} = V_{dc} \tag{1}$$

$$i_{pc} + i_o = i_{in} \tag{2}$$

The voltage v_{pc} and the voltage across the inductance L_m will depend on the state of the semiconductor switch S_1 and are given by (3) and (4), respectively, where n is the transformer's turns ratio $n = \frac{n_2}{n_1}$.

$$v_{pc} = \begin{cases} -n \cdot V_{pv} \text{ , if } S_1 \text{ ON} \\ V_{dc} - V_{pv} \text{ , if } S_1 \text{ OFF} \end{cases} \tag{3}$$

$$v_{Lm} = \begin{cases} V_{pv} \text{ , } & \text{if } S_1 \text{ ON} \\ \dfrac{V_{dc} - V_{pv}}{n} & \text{, if } S_1 \text{ OFF} \end{cases} \tag{4}$$

In Figures 3 and 4 the currents of the converter can be seen during steady-state operation. The input current i_{in} is non-linear due to being the sum of currents with different magnitudes. This gap between i_{pc} and i_o is proportional to the turns ratio of the transformer.

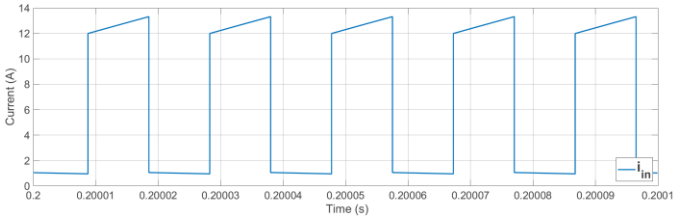

Fig. 3 – Step-up PPC current i_{in}

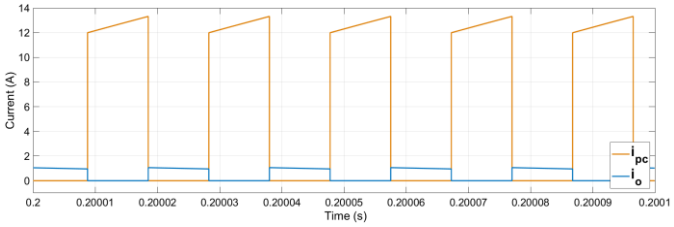

Fig. 4 – Step-up PPC current i_{pc} (orange) and i_o (blue)

$$G_{v_{flyback}} = n \cdot \frac{\delta}{1-\delta} \tag{5}$$

In order to size the PPC converter we need to derive the input/output voltage relations. For comparison, the expression for the flyback converter voltage gain is (5), where δ is the duty-cycle of the switch. The gain for the PPC converter can be calculated from the average value of the voltage in the inductance. Given that in steady-state the average voltage in the inductance is zero:

$$V_{L_m} = \frac{1}{T}\int_0^T v_{L_m} dt = 0 \Leftrightarrow$$
$$\Leftrightarrow \frac{V_{dc}}{V_{pv}} = G_{v_{PPC}} = \frac{1+\delta(n-1)}{1-\delta} \quad (6)$$

The MPP PV panel voltage, V_{mp} = 28V can be used as the nominal value since it uses the PV panel's nominal operating cell temperature of 45ºC, which is a more realistic scenario than STC conditions of 25ºC cell temperature. The output voltage will be the 380V DC grid's voltage and so the required voltage gain is:

$$G_{v_{PPC}} = \frac{V_{dc}}{V_{pv}} \quad (7)$$

Using this voltage gain as reference for the nominal operation of the converter the turns ratio of the transformer can be obtained. The desired duty-cycle δ during nominal operation should be around 50% since this is the duty-cycle that minimizes magnetic losses in the core for the flyback converter [9]. Solving (6) for n we get:

$$n = 1 + \frac{G_{v_{PPC}}(1-\delta)+1}{\delta} \quad (8)$$

The authors of [2] and [8] present a parameter to analyze the power processed by the PPC, which is simply the ratio between the power processed by the converter and the power delivered by the PV system as in (9).This parameter will be a value below unity since the converter will process less power than the power supplied by the PV system.

$$K_{pr} = \frac{P_{pc}}{P_{pv}} \quad (9)$$

To calculate the K_{pr} for this converter the power $P_{pv} = V_{pv} \cdot I_{pv}$ and $P_{pc} = V_{pv} \cdot I_{pc}$, which are the power supplied by the PV system and the power processed by the PPC respectively, are used. The efficiency of the converter is calculated in (10), where P_o is the output power of the PPC.

$$\eta = \frac{V_{dc} \cdot I_{dc}}{V_{pv} \cdot I_{pv}} = \frac{P_o}{P_{pv}} \quad (10)$$

Then substituting (10) in (9) the value of K_{pr} for this converter is obtained (11). For this converter the K_{pr} depends on the voltage gain and efficiency of the converter.

$$K_{pr} = 1 - \frac{\eta}{G_{v_{PPC}}} \quad (11)$$

The magnetizing inductance of the transformer also needs to be determined. In steady-state the average value of i_{Lm} will remain constant. However, the current waveform will present a triangular shape which is affected by the magnetizing inductance. Expression (12) is used to calculate the current ripple.

$$\Delta i_{L_m} = \frac{V_{pv} \cdot \delta \cdot T_s}{L_m} \quad (12)$$

The current ripple Δi_{Lm} in (12) still needs to be chosen in order to determine L_m. The average current in L_m will be given by (13), after adjusting for a PPC configuration with a factor of K_{pr}.

$$I_{L_m} = \frac{P_{pv}}{V_{pv} \cdot \delta} \cdot K_{pr} \quad (13)$$

Solving (12), L_m is calculated:

$$L_m = \frac{V_{pv} \cdot \delta \cdot T_s}{\Delta i_{L_m}} \quad (14)$$

The sizing of the input capacitor takes into account the current ripple in i_{in} which is a non-linear current due to it switching between windings (Fig. 3). Applying Kirchhoff's Current law, i_{Cpv} is given by (15) and its waveform can be seen in Fig. 5.

$$i_{Cpv} = i_{pv} - i_{in} \quad (15)$$

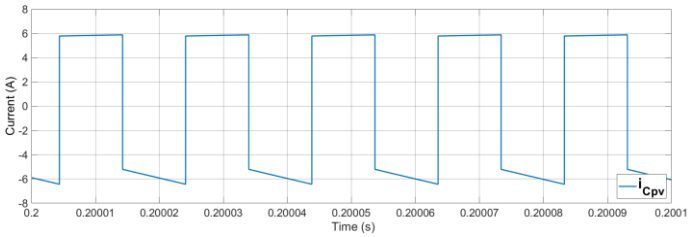

Fig. 5 - Current i_{Cpv}

Since current i_{pv} is a slow changing current with a small ripple, it's only needed to determine the ripple of current i_{in}, which is given by (16) and (17).

$$i_{in} = \begin{cases} i_{L_m}, \text{ if } S_1 \text{ ON} \\ \frac{i_{L_m}}{n}, \text{ if } S_1 \text{ OFF} \end{cases} \quad (16)$$

$$\Delta i_{in} = I_{L_m} + \frac{\Delta i_{L_m}}{2} - \frac{I_{L_m} - \frac{\Delta i_{L_m}}{2}}{n} \quad (17)$$

The output capacitor will be sized assuming steady state operation and so it can be given by expression (18):

$$C_{pv} = \frac{I_{Cpv} \cdot \delta \cdot T_s}{\Delta V_{pv}} \tag{18}$$

Even though the average value of current i_{Cpv} is zero in steady state, it oscillates around zero with a peak-to-peak amplitude of Δi_{in} and its waveform somehow resembles a square waveform. For the purpose of sizing the input capacitor, i_{Cpv} is approximated to a square waveform centered in zero and with a value of $\Delta i_{in}/2$ when S_1 is ON and $-\Delta i_{in}/2$ when S_1 is OFF. Assuming a maximum ripple of 2% in V_{pv}, C_{pv} can be calculated by the following equation:

$$C_{pv} = \frac{\frac{\Delta i_{in}}{2} \cdot \delta \cdot T_s}{\Delta V_{pv}} \tag{19}$$

In table 1 all the relevant calculated parameters for the step-up PPC can be found.

Table 1 - Step-up PPC nominal operation parameters

Nominal Operation Parameters	
Input Voltage V_{pv} [V]	28
Input Current I_{pv} [A]	6.7
Output Voltage V_{dc} [V]	380
Output Current I_{dc} [A]	0.48
Duty-cycle [%]	50
Switching frequency f_s [kHz]	50
Partial power ratio K_{pr}	0.9263
Transformer's turns ratio, n	12.57
Magnetizing inductance L_m [µH]	225
Input capacitor C_{pv} [µF]	108

III. Controllers Design

In this chapter the control strategies used for the step-up PPC are developed. For all the converters, nonlinear control methods are used and for the step-up PPC a linear PI controller is designed for comparison purposes [10].

The converters studied in this paper are all nonlinear systems. This requires the system to be linearized to apply classical control methods. The problem with this linearization is that it is done for a certain operation point and for large deviations from this point the controller's performance worsens. An alternative is to use non-linear control methods as the backstepping technique and sliding mode control. Both these methods are used to design the controllers of the converters along with the use of Lyapunov's second method to assure the stability of the system [11] [12].

1) Step-up PPC non-linear control

The nonlinear controller developed for the step-up PPC uses an external loop for the voltage using the backstepping technique and internal loop for current using sliding mode control.

a) Backstepping voltage controller

The voltage to be controlled in the step-up PPC is the PV panel voltage, which is the input voltage of the converter (Fig. 2). The error e_{Vpv} is then defined as:

$$e_{Vpv} = V_{PVref} - V_{pv} \tag{20}$$

The integral error of the voltage is also defined:

$$e_{I1} = \int_0^t e_{Vpv}\, dt \tag{21}$$

The integral error is used to assure zero steady-state error that may occur due to parameters mismatch. Combining the two errors a Lyapunov function is proposed:

$$V_{v1} = K_{I1}\frac{e_{I1}^2}{2} + \frac{e_{Vpv}^2}{2}\ ,\ K_{I1} > 0 \tag{22}$$

Where K_{I1} is a constant greater than zero. This function is positive definite and radially bounded. Its time derivative is:

$$\dot{V}_{v1} = K_{I1} \cdot e_{I1} \cdot e_{Vpv} + e_{Vpv}\frac{de_{Vpv}}{dt} \tag{23}$$

To guarantee asymptotic stability Lyapunov's second method is used and the following constraint is applied:

$$\begin{gathered} \dot{V}_{v1} < 0 \Rightarrow \\ \Rightarrow K_{I1}e_{I1}e_{Vpv} + e_{Vpv}\frac{de_{Vpv}}{dt} = -K_{v1}e_{Vpv}^2\ ,\ K_{v1} > 0 \end{gathered} \tag{24}$$

The time derivative of the input voltage is:

$$\frac{dV_{pv}}{dt} = \frac{i_{Cpv}}{C_{pv}} = \frac{i_{pv} - i_{in}}{C_{pv}} \tag{25}$$

Using (25) the time derivative of the error e_{Vpv} is obtained:

$$\frac{de_{Vpv}}{dt} = \frac{dV_{PVref}}{dt} - \frac{i_{pv} - i_{in}}{C_{pv}} \tag{26}$$

By using (26) in (24) and solving for the current i_{in} the control law for that current is obtained:

$$I_{INref} = i_{pv} - C_{pv}\left(K_{v1}e_{Vpv} + K_{I1}e_{I1} + \frac{dV_{PVref}}{dt} \right) \tag{27}$$

b) Sliding mode current controller

The inner loop controls the input current of the converter and uses sliding mode control. Since the control objective is i_{in}=I_{INref} , the sliding surface of the controller is the error associated with this current, which is to be kept in the vicinity of zero.

$$s(i_{in}) = e_{in} = I_{INref} - i_{in} \tag{28}$$

In order to determine the control law, the dynamics of the input current i_{in} is calculated using (4) and (16) resulting in (29).

$$\frac{di_{in}}{dt} = \begin{cases} \frac{di_{L_m}}{dt} = \frac{v_{pv}}{L_m} , & \text{if } S_1 \text{ ON} \\ \frac{\frac{di_{L_m}}{dt}}{n} = \frac{v_{pv} - v_{dc}}{n^2 L_m} , & \text{if } S_1 \text{ OFF} \end{cases} \tag{29}$$

As the DC grid voltage, v_{dc}, is always higher than the PV voltage, v_{pv}, the derivative of the input current has different signs according to the state of the semiconductor switch:

$$\begin{cases} \frac{di_{in}}{dt} > 0 \Rightarrow \frac{de_{Iin}}{dt} < 0 , \text{ if } S_1 \text{ ON} \\ \frac{di_{in}}{dt} < 0 \Rightarrow \frac{de_{Iin}}{dt} > 0 , \text{ if } S_1 \text{ OFF} \end{cases} \tag{30}$$

From (30) the state of the semiconductor can be chosen in order to satisfy condition $e_{Iin} \cdot \frac{de_{Iin}}{dt} < 0$:

$$\begin{cases} e_{Iin} > 0 \rightarrow \frac{de_{Iin}}{dt} < 0 \rightarrow S_1 \text{ ON} \\ e_{Iin} < 0 \rightarrow \frac{de_{Iin}}{dt} > 0 \rightarrow S_1 \text{ OFF} \end{cases} \tag{31}$$

The system cannot reach the surface otherwise the switching frequency would need to be infinite. An interval centered around zero must be determined.

As was shown in Fig. 3 the input current is discontinuous as the result of being the sum of the two winding currents of the transformer. Consequently, when the state of the semiconductor switch changes the current suffers a significant discontinuous increase/decrease. The difference of magnitude between the winding currents of the transformer increases as turns ratio increases. This difference is reflected in current i_{in} and must be accounted for. Specifically, the acceptable error interval needs to include the difference between the winding currents.

Considering the upper boundary of the current, it must be high enough so that when it is divided by the transformer turns ratio it is still higher than the lower boundary. This results in the condition (32) where the minimum ratio d, for which the current reference can be multiplied, is obtained.

$$\begin{aligned} \frac{I_{INref} + I_{INref}\frac{d}{2}}{n} \geq I_{INref} - I_{INref}\frac{d}{2} \Leftrightarrow \\ \Leftrightarrow d \geq 2\frac{n-1}{n+1} \end{aligned} \tag{32}$$

A minimum error ripple is defined as $\Delta_{min} = I_{INref} \cdot d$. This ripple is then increased $\Delta = \Delta_{min} + \Delta_{add}$, through the use of the term Δ_{add} to match the desired switching frequency, in this case 50 kHz for nominal operation of the PV panel. Finally the control law is obtained as presented in (33):

$$\begin{cases} e_{Iin} > \frac{\Delta}{2} \rightarrow \frac{de_{Iin}}{dt} < 0 \rightarrow S_1 \text{ ON} \\ e_{Iin} < -\frac{\Delta}{2} \rightarrow \frac{de_{Iin}}{dt} > 0 \rightarrow S_1 \text{ OFF} \end{cases} \tag{33}$$

Regarding the switching frequency it must also be noted that as the PV panel deviates from nominal operation so will its current, meaning that if the irradiance lowers, i_{pv} lowers as well. Consequently, the current reference also lowers as a result, and the error ripple gets smaller, which will increase the switching frequency.

IV. RESULTS

The operation of the sized converters and designed controllers will be analyzed in order to evaluate their performance. Using *MatLab/Simulink* the elements in Fig. 1 were modelled and tested in different operation scenarios:

- Scenario 1 – Stand-alone operation of PV panel in nominal conditions
- Scenario 2 – Stand-alone operation of PV panel with irradiance levels change
- Scenario 3 – DC grid behaviour

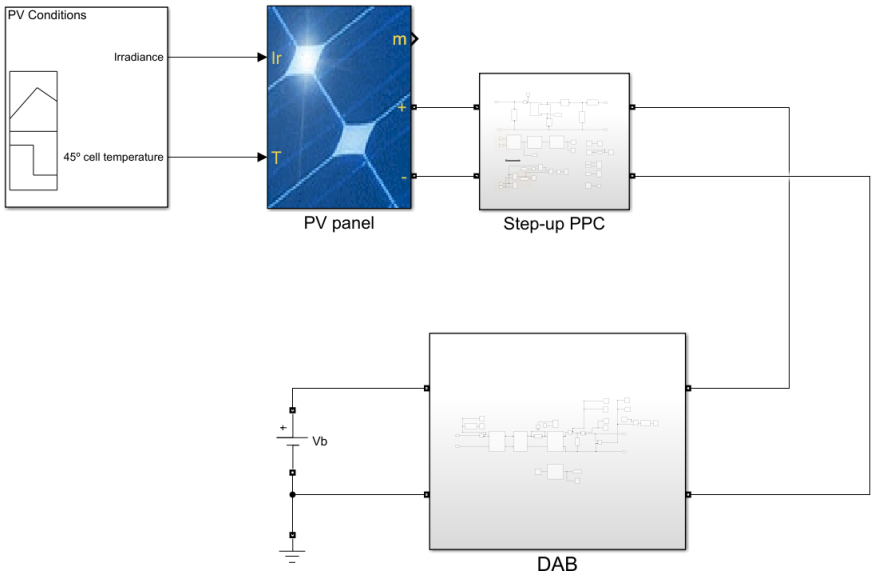

Fig. 6 – *Matlab/Simulink* model used for scenario 1 and 2.

A. *Scenario 1 - PV panel operation in nominal conditions*

The first scenario tested focuses on the PV system working at nominal conditions which are: an irradiance of 800 W/m^2 and a cell temperature of 45 C^o. These are called Nominal Operating Cell Temperature (NOCT) conditions. In these conditions the panel operates at its MPP if its voltage is 28V and is supplying a power of around 188W. The operating values in NOCT conditions for this PV panel are seen in table 2.

Table 2 – PV panel manufacturer's datasheet data for NOCT conditions

Maximum power P_{mp} [W]	188
MPP current I_{mp} [A]	6.7
MPP voltage V_{mp} [V]	28
I_{SC} [A]	7.28
V_{OC} [V]	34.7

The connection of the PV system is made using the step-up PPC and its simulation parameters are the same ones presented in table 1. In Fig. 6 the *MatLab/Simulink* model used to test scenario 1 and 2 is shown.

The results from using the non-linear controller design in section III.1) are presented in Fig. 7 where both the PV voltage and MPPT voltage reference are shown. It is clear that the PV voltage has reached the desired MPP of 28V and it is oscillating around this value, as is expected from the P&O method. The controller is able to make the PV voltage follow the MPPT voltage reference for a MPPT period of 5 ms with a fast response and while attenuating any oscillations.

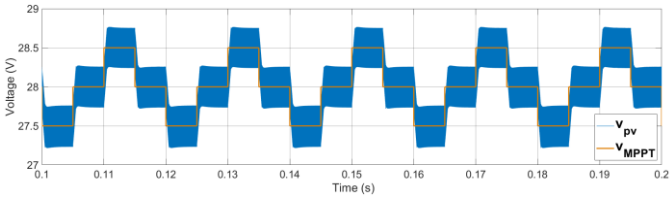

Fig. 7 - Voltage MPPT tracking using a non-linear controller during nominal operation

Furthermore, the power generated by the PV panel is seen in Fig. 8. It is slightly above 188W, around 191W, and this may be due to a mismatch between the actual values from the PV panel datasheet and the ones used in the *Simulink* model. Nonetheless the values are close enough to conclude that it is working correctly. It can be noted that the slight oscillation observed in the power is due to the voltage level being constantly oscillating around 28V. The partial power ratio K_{pr} also presents this oscillation (Fig. 9) but matches the expected value, averaging at $K_{pr} \approx 0.9265$, very close to the 0.9263 theoretical value.

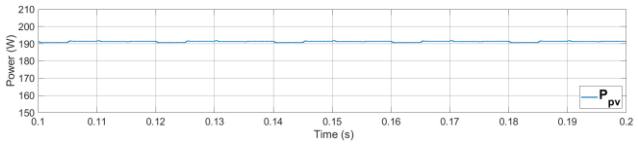

Fig. 8 - Input PV power P_{pv}

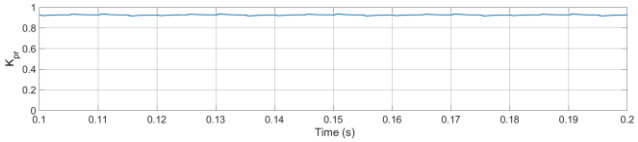

Fig. 9 - Partial power ratio K_{pr} of the step-up PPC during nominal operation

A comparison of losses between the step-up PPC and the flyback converter is also made because of their similarities. Conduction losses are accounted for all of the converters elements and so are the switching losses for the MOSFET semiconductor. It must be noted that the *Simulink* model of the semiconductors is ideal, so a parallel RC circuit is added to simulate switching losses, sized for a turn-on and turn-off time of 100 ns. The flyback converter that is used as comparison is sized to work at the same conditions as the step-up PPC. In table 3 the parameters used to model the conduction losses are displayed. Except for the transformer's winding resistances and input capacitor resistance, which are sized for 0.5% of the input power in losses, all the parameters were taken from datasheets of components appropriate to work at the voltages and currents of the system at nominal operation. The transformer of the step-up PPC was also sized for a fraction of the input power, equal to the partial power ratio K_{pr} = 0.9263, effectively reducing the conduction losses.

Table 3 - Non ideal elements used to model conduction losses in both converters.

PPC primary winding resistance R_1 [mΩ]	10
Flyback primary winding resistance R_{1fb} [mΩ]	11
PPC secondary winding resistance R_2 [mΩ]	126
Flyback secondary winding resistance R_{2fb} [mΩ]	150
Input capacitor resistance R_c [Ω]	30
MOSFET ON resistance R_{ds} [Ω]	17
Diode resistance R_d [Ω]	21.5
Diode forward voltage V_d [V]	0.9

The MPPT algorithm is turned off for this comparison of losses and instead the non-linear voltage controller is given a constant voltage reference of 28V. This will eliminate the oscillation of the voltage value around 28V and make it easier to compare the values between the converters. For each converter (step-up PPC and flyback) the power being generated by the PV system is measured as well as the output power, then the efficiency of the converter is computed. The results are seen in Fig. 10 and Fig. 11 for the step-up PPC and Flyback converter, respectively.

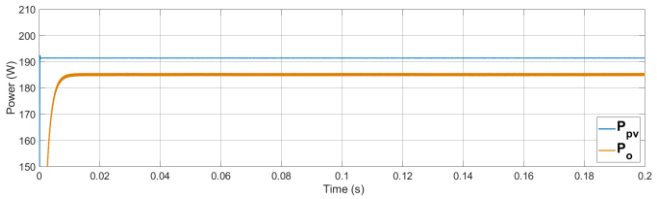

a) Input PV power P_{pv} (blue) and output power P_o (orange).

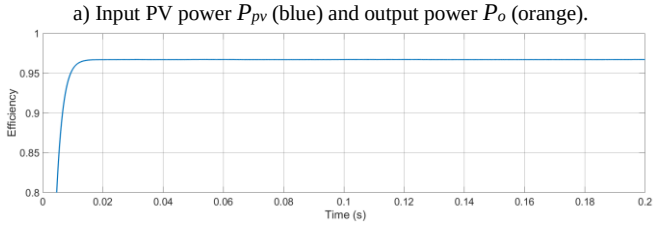

b) Efficiency

Fig. 10 - Input power, output power and efficiency for nominal operation of the step-up PPC considering conduction and switching losses

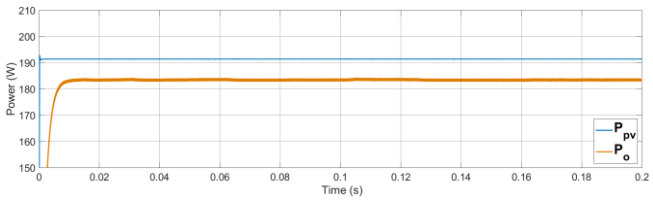

a) Input PV power P_{pv} (blue) and output power P_o (orange).

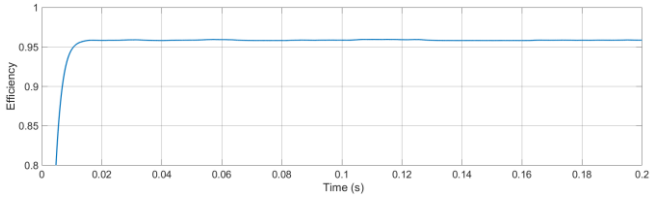

b) Efficiency

Fig. 11 - Input power, output power and efficiency for nominal operation of the Flyback converter considering conduction and switching losses

While in both cases the input power was the same, P_{pv}=191.6W, the output power differed. The step-up PPC reached an output power of P_o=185.2W and efficiency of η=96.7% whereas the flyback converter reached an output power of P_o=183.6W and efficiency of η=95.8%. The voltage and currents in the semiconductors also differ. The K_{pr} also slightly increased in the step-up PPC when losses were simulated because it depends on the efficiency of the converter and it was previously simulated without considering them. Table 4 summarizes the differences between the converters, including the voltage and current levels in the semiconductors. In comparison to the flyback converter the step-up PPC is able to achieve a better efficiency while also reducing the semiconductors ratings.

Table 4 - Differences between step-up PPC and flyback at nominal operation

Parameter	Step-up PPC	Flyback
Input Power [W]	191.6	191.6
Output Power [W]	185.2	183.6
Efficiency [%]	96.7	95.8
MOSFET blocking voltage [V]	56	56
MOSFET draining current [A]	6.35	6.83
Diode blocking voltage [V]	700	756
Diode forward current [A]	0.48	0.48

B. Scenario 2 - PV panel operation with irradiance levels change

The second scenario is still focused in the PV system, however in this case the irradiance levels change during the simulation in order to evaluate if the system is able to respond to these changes, namely if the PV panel maintains its MPP operation. The *MatLab/Simulink* model for this scenario is the one seen in

Fig. 6 since the focus is still in the connection of the PV system to the DC microgrid.

The irradiance levels change in the following order:

- Instant t = 0s : Irradiance = 600 W/m^2
- Instant t = 0.2s : Irradiance = 800 W/m^2
- Instant t = 0.4s : Irradiance = 400 W/m^2
- Instant t = 0.6s : Irradiance = 200 W/m^2

Each irradiance level lasts for 0.2s for a total test duration of 0.8s. In Fig. 12 the results for using the nonlinear controller are presented. The controller is able to maintain the MPPT for all irradiances. The voltage reference, v_{MPPT}, oscillates around the value of 28V for all irradiance levels except the last one of 200 W/m^2 where it dropped to 27.5V.

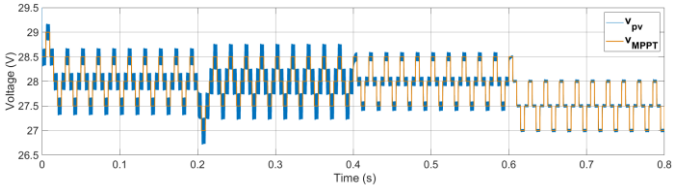

Fig. 12 - Voltage MPPT tracking using a non-linear controller for various irradiance levels

Figures 13 and 14 show the power generated by the PV system and the partial power ratio respectively, for the various irradiance levels while using the nonlinear controller. The results are as expected, with the power generated by the PV system being proportional to the irradiance level and the partial power ratio of the step-up PPC remaining mostly constant (besides the disturbances that occur when the irradiance is changed). The partial power ratio should remain constant for the different irradiances since it depends on the voltage gain of the converter, which remains the same for all the irradiances except for the last one of 200 W/m^2.

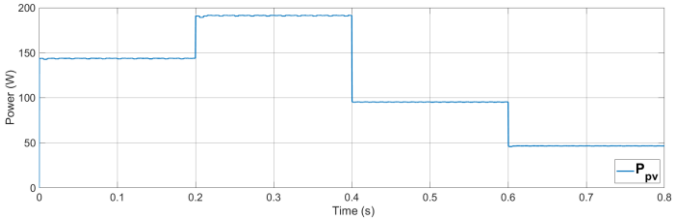

Fig. 13 - Input PV power P_{pv} for the various irradiance levels

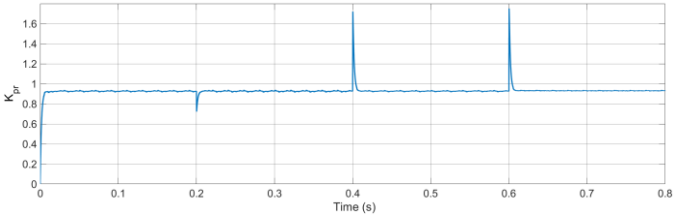

Fig. 14 - Partial power ratio K_{pr} of the step-up PPC for various irradiance levels

Table 5 compiles the results of this scenario while using the nonlinear controller. The switching frequency is also measured since it changes according to the irradiance level, as explained in section III.1)b). The switching frequency is 50 kHz for the 800 W/m^2 and it increases up to 112 kHz at 200 W/m^2, so even though the nonlinear controller is able to follow the voltage reference in low irradiance conditions, the converter is working at a switching frequency higher than the one the converter was designed for.

Table 5 - Results for the scenario 2 test

Irradiance [W/m^2]	800	600	400	200
MPP voltage [V]	28	28	28	27.5
Input PV power P_{pv} [W]	191	144	95	47
Partial power ratio K_{pr} [%]	92.6	92.6	92.6	92.6
Switching frequency f_s [kHz]	50	57	70	112

C. Scenario 3 - DC grid behavior when both PV panel and CPLs are connected and disconnected

The third scenario is aimed at observing the DC microgrid behavior, namely its voltage and current, when both the PV system and CPLs are connected, disconnected or working simultaneously. This scenario includes all of the DC microgrid elements represented in Fig. 1 and its *MatLab/Simulink* model can be seen in Fig. 15. The design, sizing and control of the step-down PPC and DAB converter were done in this dissertation [10] but the results for this scenario are show hereafter.

As the DAB converter is responsible for setting and maintaining the DC microgrid voltage v_{dc} and balancing the power flow, its output current i_g is indicative if the DAB converter is either consuming or generating power. A negative value of i_g means power is being consumed while a positive value means the DAB is generating power.

The test has a duration of 0.3s and consists of the following steps:

- Instant t = 0s : PV system is connected at NOCT conditions: Irradiance = 800 W/m^2 and a 45 C^o cell temperature
- Instant t = 0.1s : 200W/24V load is connected
- Instant t = 0.2s : PV system is disconnected and 300W/48V load is connected

The test consists of three periods where the power processed by the DAB converter is different. Until t = 0s only the PV system is connected and so the DAB converter must consume all of its power (current i_g must be negative). From t = 0.1s until t = 0.2s both the PV system and 200W load are connected and since the PV system generates almost 200W in NOCT conditions the

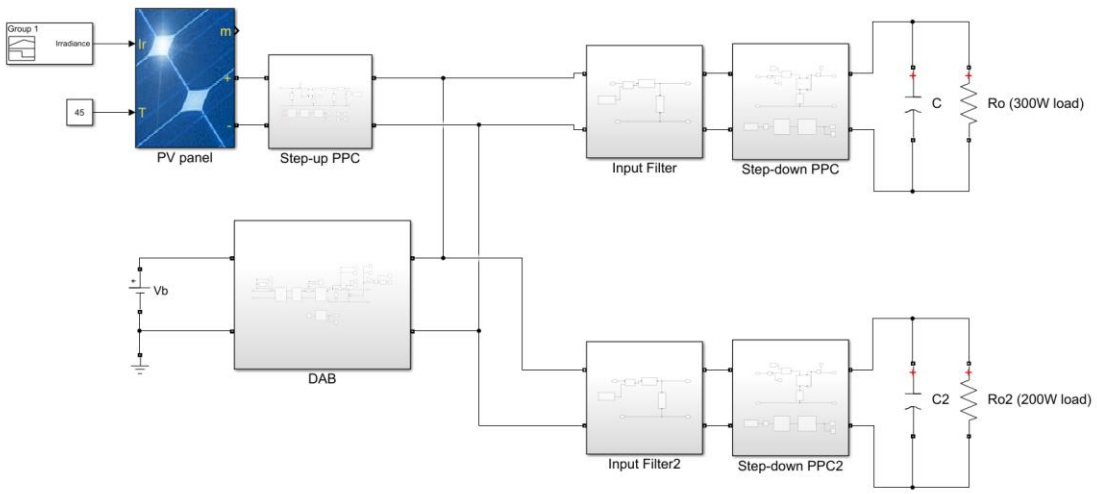

Fig. 15 - *Matlab/Simulink* model used for scenario 3.

DAB converter will work at low power (current i_g must be close to zero). Finally, at t = 0.2s the PV system is disconnected and the 300W load is connected. This amounts to a total power being consumed of 500W (current i_g should be positive).

In Fig. 16 the voltage and current at the output of DAB converter can be seen. Except for a small dip after connecting the 300W load the output voltage remained close to the value of 380V for the duration of the test. On the other hand, the current presents two spikes which are caused by the charging of the input filters of the step-down PPCs when they are connected at t = 0.1s and t = 0.2s.

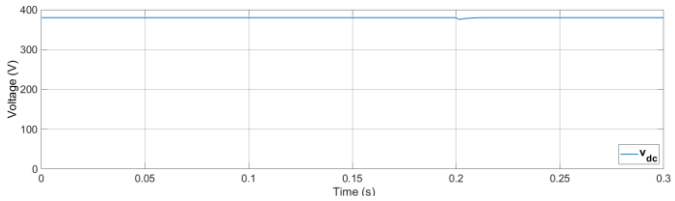

a) DC microgrid voltage v_{dc}

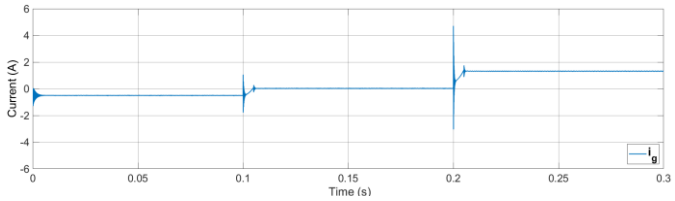

b) DAB converter output current i_g

Fig. 16 - DC microgrid voltage and current during scenario 3 test

Observing Fig. 16 and Fig. 17 confirms that the DAB converter is working correctly in the three different zones. First it consumes around 190W and its current is negative, in the following zone both its power and current are close to zero because the PV system power closely matches the load's power and lastly the DAB generates 500W and its current is positive.

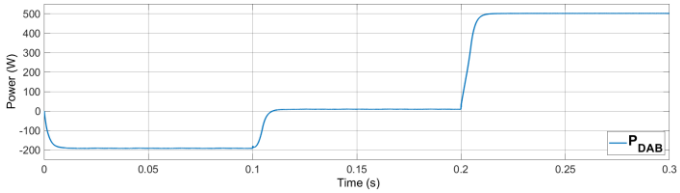

Fig. 17 - Power being processed by the DAB converter

The voltages of the PV system and the loads are presented in Fig. 18, where the MPPT can be seen working in the PV voltage as well as the soft-starters for the step-down PPCs.

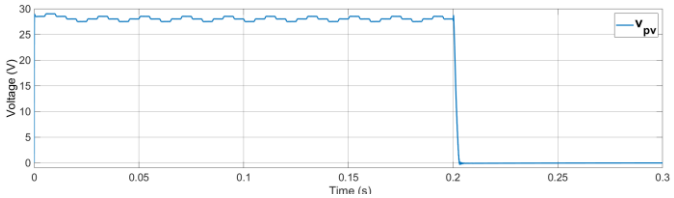

a) PV voltage v_{pv}

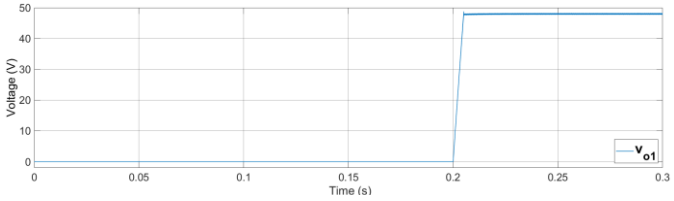

b) Output voltage v_{o1} for the 48V load

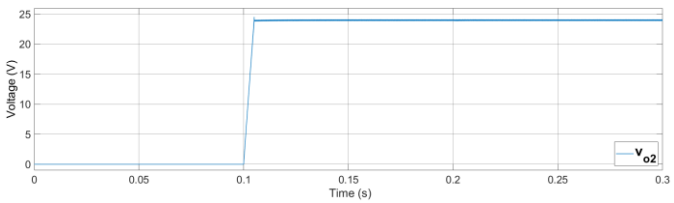

c) Output voltage v_{o2} for the 24V load

Fig. 18 - PV voltage and load output voltages during scenario 3 test

The DAB converter proved to be a suitable converter guaranteeing bidirectional power flow. Due to the non-linear

controllers the DC microgrid robustness to changes in operating conditions is achieved, maintaining the DC microgrid voltage stable while both generation of power and consumption occurred. Additionally, the results of this scenario show that all the elements of the DC microgrid are sized appropriately and the desired behavior of the DC microgrid is achieved.

V. Conclusion

The main objective of this paper was to study a converter topology, based on the technique of partial power processing, in the context of a DC grid and analyze if its performance, present its benefits over existing converters, namely a better efficiency and a reduction in the power ratings of the converter's components. This converter topology was originally proposed as the DC-DC stage of the connection of a PV system to an AC grid, but in the case of connection to a DC grid its use is even more justified since no AC-DC stage is needed.

A DC microgrid was modelled and simulated in *Matlab/Simulink* where various scenarios were tested. The obtained results were satisfactory and were the expected ones: the step-up PPC connected the PV panel to the DC microgrid while obtaining a better efficiency and lower power ratings for its components in comparison to the similar and commonly used flyback converter; the non-linear controllers were shown to have a fast response and able to easily attenuate oscillations.

VI. References

[1] R. M. Button, "An advanced photovoltaic array regulator module," in *Proceedings of the 31st Intersociety Energy Conversion Engineering Conference*, IECEC 96, 1996.

[2] J. W. Zapata, S. Kouro, G. Carrasco, H.Renaudineau and T. A. Meynard, "Analysis of partial power DC-DC converters for two-stage photovoltaic systems," *IEEE Journal of Emerging and SelectedTopics in Power Electronics,* vol. 7, no. 1, pp. 591-603, 2019.

[3] J. Anzola, I. Aizpuru, A. A. Romero, A. A. Loiti, R. Lopez-Erauskin, J. S. Artal-Sevil and C. Bernal, "Review of architectures based on partial power processing for DC-DC applications," *IEEE Access,* vol. 8, pp. 103405-103418, 2020.

[4] M. Kasper, D. Bortis and J. W. Kolar, "Classification and comparative evaluation of PV panel-integrated DC-DC converter concepts," *IEEE Transactions on Power Electronics,* vol. 29, no. 5, pp. 2511-2526, 2014.

[5] S. Muller, M. Deicke and R. W. D. Doncker, "Doubly fed induction generator systems for windturbines," *IEEE Industry Applications Magazine,* vol. 8, no. 3, pp. 26-33, 2002.

[6] A. G. Birchenough, "A high efficiency DC bus regulator / RPC for spacecraft applications," *AIP conference proceedings,* vol. 699, pp. 606-613, 2004.

[7] M. S. Agamy, M. Harfman-Todorovic, A. Elasser, S. Chi, R. L. Steigerwald, J. A. Sabate, A. J.McCann, L. Zhang and F. J. Mueller, "An efficient partial power processing DC/DC converter for distributed PV architectures," *IEEE Transactions on Power Electronics,* vol. 29, no. 2, pp. 674-686, 2014.

[8] J. W. Zapata, H. Renaudineau, S. Kouro, M. A. Perez and T. A. Meynard, "Partial power DC-DC converter for photovoltaic microinverters," *IECON 2016 - 42nd Annual Conference of the IEEEIndustrial Electronics Society,* pp. 6740-6745, 2016.

[9] M. Albach, T. Durbaum and A. Brockmeyer, "Calculating core losses in transformers for arbitrary magnetizing currents a comparison of different approaches," *PESC Record. 27th Annual IEEE Power Electronics Specialists Conference,* vol. 2, pp. 1463-1468, 1996.

[10] J. Campos, "Partial power DC-DC converter to integrate PV systems in DC grids," Master's Thesis, Instituto Superior Técnico, Universidade de Lisboa, Dec. 2020.

[11] H. K. Khalil, Nonlinear systems, 3rd ed., New Jersey, USA: Prentice Hall, 2002.

[12] G. M. Paraíso, "Design of control strategies for low voltage DC residential grids," Master's Thesis, Instituto Superior Técnico, Universidade de Lisboa, Nov. 2018.